Kumar et al. Nanoscale Research Letters (2016) 11:434
DOI 10.1186/s11671-016-1657-5

Nanoscale Research Letters

NANO EXPRESS Open Access

Detection of pH and Enzyme-Free H_2O_2 Sensing Mechanism by Using GdO_x Membrane in Electrolyte-Insulator-Semiconductor Structure

Pankaj Kumar[1], Siddheswar Maikap[1,2,3*], Jian-Tai Qiu[4,5], Surajit Jana[1], Anisha Roy[1], Kanishk Singh[1], Hsin-Ming Cheng[6], Mu-Tung Chang[6], Rajat Mahapatra[7], Hsien-Chin Chiu[1] and Jer-Ren Yang[8]

Abstract

A 15-nm-thick GdO_x membrane in an electrolyte-insulator-semiconductor (EIS) structure shows a higher pH sensitivity of 54.2 mV/pH and enzyme-free hydrogen peroxide (H_2O_2) detection than those of the bare SiO_2 and 3-nm-thick GdO_x membranes for the first time. Polycrystalline grain and higher Gd content of the thicker GdO_x films are confirmed by transmission electron microscopy (TEM) and X-ray photo-electron spectroscopy (XPS), respectively. In a thicker GdO_x membrane, polycrystalline grain has lower energy gap and Gd^{2+} oxidation states lead to change Gd^{3+} states in the presence of H_2O_2, which are confirmed by electron energy loss spectroscopy (EELS). The oxidation/reduction (redox) properties of thicker GdO_x membrane with higher Gd content are responsible for detecting H_2O_2 whereas both bare SiO_2 and thinner GdO_x membranes do not show sensing. A low detection limit of 1 μM is obtained due to strong catalytic activity of Gd. The reference voltage shift increases with increase of the H_2O_2 concentration from 1 to 200 μM owing to more generation of Gd^{3+} ions, and the H_2O_2 sensing mechanism has been explained as well.

Keywords: Enzyme-free H_2O_2, pH detection, GdO_x, Sensing mechanism, Catalytic, EIS structure

Background

Recently, hydrogen peroxide (H_2O_2) is a major intermediate of biological cycles which has been used as a potential biomarker for oxidative stress diagnosis as well as a major catalyst for immune sensing [1, 2]. On the other hand, it is also an essential compound of bleach industries and waste water treatment. H_2O_2 has a major role in modulating mitochondrial function by inhibiting activities of the mitochondrial enzyme in a fully reversible fashion [3, 4]. The H_2O_2 sensing assay relies on the use of the enzyme horse radish peroxidase (HRP) to oxidize its substrates and detection using spectrophotometer [5]. H_2O_2 sensing in a simple way, with a short time detection with high specificity, is demanded for future disease diagnosis of the human body, and enzyme-free electro-catalytic methods have gained the attention for H_2O_2 sensing. Therefore, various catalysts such as metal, metal oxides, and redox polymers have been reported to detect H_2O_2 [6–12]. Huang et al. [13] have used the glassy carbon electrode modified by Si nanowire-dispersed CuO nanoparticle. Maji et al. [14] have demonstrated an amperometric H_2O_2 sensor based on reduced graphene oxide-coated silica modified with Au nanoparticles. Wang et al. [15] have developed a H_2O_2 sensor by using MoS_2 nanoparticles. Sun et al. [16] have reported a dumbbell-like Pt-Pd-Fe_3O_4 nanoparticle-modified glassy carbon electrode which shows electro-catalytic reduction. Liu et al. [17] have reported an amperometric H_2O_2 sensor based on a Si substrate modified with carbon nanotube microelectrode coated by Pd nanoparticles. Kong et al. [18] have reported a non-enzymatic H_2O_2 sensor based on a Co_3O_4 nanowire

* Correspondence: sidhu@mail.cgu.edu.tw
[1]Department of Electronic Engineering, Chang Gung University (CGU), 259 Wen-Hwa 1st Rd., Kwei-Shan, Tao-Yuan 333, Taiwan
[2]Bio-Sensor Lab., Biomedical Engineering Research Center, Department of Electronic Engineering, Chang Gung University, Tao-Yuan 333, Taiwan
Full list of author information is available at the end of the article

grown over a reduced graphene oxide sheet. Hao et al. [19] have developed an amperometric H_2O_2 sensor based on Fe_2O_3 nanoparticles. Bai et al. [20] have reported a sensor based on carbon dot-decorated multi-walled carbon nano-composites. Silver (Ag) nanowire [21] and nanoparticle-decorated graphene [22] have been also reported for H_2O_2 sensing. Most of the above groups have used different materials using cyclic voltammetry/amperometric methods to sense H_2O_2 (ranging from few nanomolars to millimolars) due to different oxidation states in the presence of H_2O_2. On the other hand, high-k materials such as Al_2O_3 [23], Ta_2O_5 [24], and HfO_2 [25] in an electrolyte-insulator-semiconductor (EIS) structure have been reported for pH sensing only; however, the Gd_2O_3 materials that have been reported are few [26, 27], and even then, there is no report for enzyme-free H_2O_2 sensing by using a GdO_x ($x < 1.5$) material in a simple EIS structure. In this paper, detection of a pH and enzyme-free H_2O_2 sensing mechanism has been investigated by using a GdO_x membrane in a simple EIS structure for the first time. Polycrystalline grain, Gd content, and oxidation states (Gd^{2+}/Gd^{3+}) have been confirmed by transmission electron microscope (TEM), X-ray photo-electron spectroscopy (XPS), and electron energy loss spectroscopy (EELS) on grain and boundary regions. The 15-nm-thick GdO_x membrane detects H_2O_2 whereas both 3-nm-thick GdO_x and bare SiO_2 membranes do not sense H_2O_2. Due to the strong catalytic activity of Gd, a low detection limit of 1 μM is obtained. Both time- and concentration-dependent H_2O_2 sensing and its mechanism have been investigated.

Methods

p-type 4-in. Si (100) wafer was cleaned by the Radio Corporation of America (RCA) process. Prior to thermal growth of SiO_2, HF dip was used to remove native oxide from the surface. After the cleaning process, a 40-nm-thick SiO_2 layer was grown as an insulating layer by dry oxidation process at 950 °C. Then, the back-side-grown SiO_2 layer was removed by using a buffer oxide etching (BOE) solution. To fabricate the EIS chip, a 300-nm-thick Al film was deposited on the back side of the Si wafer. The sensing membrane area was defined by standard photolithography process using a negative photoresist-SU8. Then, EIS devices were attached on a printed circuit board having copper lines. An epoxy layer was used to encapsulate the EIS structure and the copper line. Therefore, a sensor (S1) using SiO_2 membrane was fabricated. Our fabrication process of EIS structure can be found elsewhere [28]. This SiO_2 sensing membrane was modified by deposition of 3-nm- (S2) and 15-nm-thick (S3) GdO_x films. The GdO_x film was deposited by electron beam evaporation. The Gd_2O_3 granules were used during deposition, and the deposition rate was 6 nm/min. A schematic view of the Gd_2O_3- (or GdO_x ($x < 1.5$)) modified SiO_2 sensor is shown in Fig. 1. To probe the thickness and microstructure of GdO_x films, low-voltage spherical aberration corrected field emission TEM (Cs-corrected FE-TEM) was performed. The model number is JEOL JEM-ARM200F with accelerating voltages of 60, 120, and 200 kV. In addition, a Cs-corrected FE-TEM Oxford energy spectrometer (energy-dispersive spectroscopy, EDS) and electron loss EDS (EELS, Model 965 QuantumER^{TM}) were used to observe the elemental composition on polycrystalline grain and boundaries. The ambient temperature of our laboratory was 21 ± 3 °C and relative humidity was 50 ± 10 %. The elemental composition was investigated by XPS analyzing chamber. The vacuum of the XPS chamber was 1×10^{-9} Torr. The spectra were recorded by using an Al K∝ monochrome X-ray at an energy of 1486.6 eV. The scanning energy range from 0 to 1350 eV was used. All spectra were calibrated by *C1s* spectrum at a centered peak energy of 284.6 eV. After depositing the GdO_x films on the SiO_2/Si substrates, the samples were transferred immediately to the XPS chamber. The capacitance-voltage (C-V) measurements were performed by using Agilent 4284A LCR meter and an Ag/AgCl reference electrode was used. The measurement frequency was 100 Hz. The sweep voltage was applied on the Ag/AgCl electrode. The reference voltage (V_r) was measured at 50 % of accumulation capacitance.

Results and Discussion

Figure 2 shows the cross-sectional TEM images of the S2 and S3 sensors. The thickness of SiO_2 is 41.2 nm (Fig. 2a), and the thickness of the GdO_x film is 3.3 nm (Fig. 2b). The TEM image of the S3 sensor shows that the thickness of SiO_2 is 41.5 nm (Fig. 2c) and the

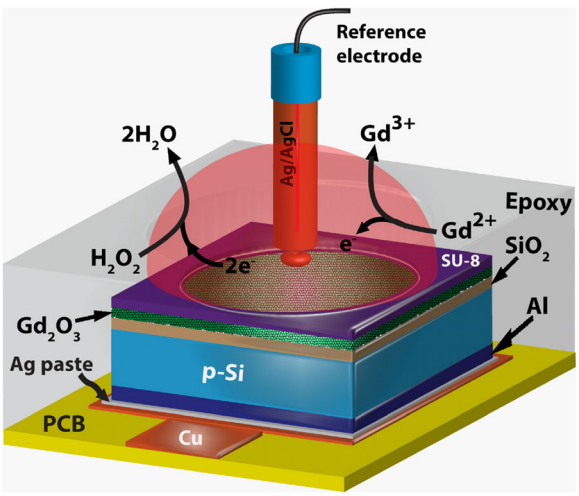

Fig. 1 Schematic view of our pH and H_2O_2 sensor using Gd_2O_3 (or GdO_x ($x < 1.5$)) membrane and demonstration of H_2O_2 sensing mechanism

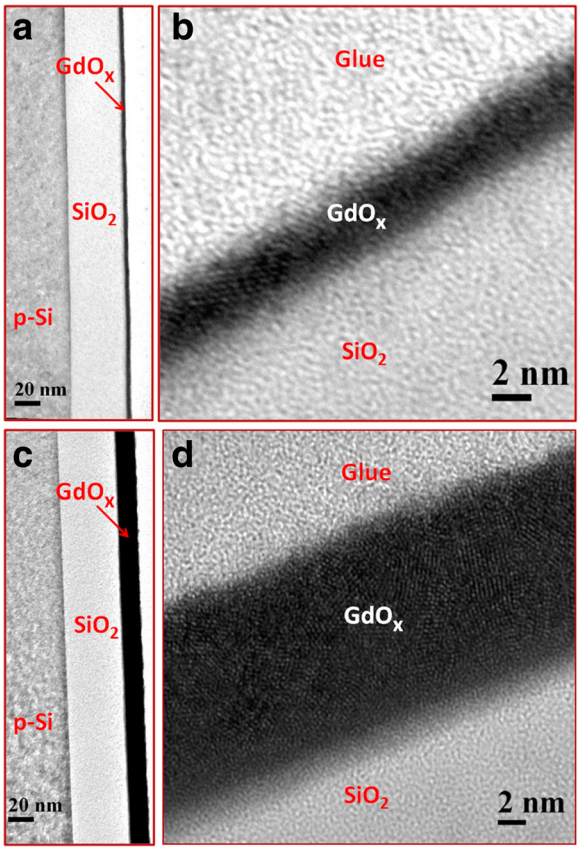

Fig. 2 TEM images of **a** 3-nm-thick GdO_x membrane on 40-nm-thick SiO_2 layer (S2) and **b** zoom in view of a. TEM images of **c** 15-nm-thick GdO_x membrane (S3) and **d** zoom in view of c. Thicker membrane shows clear polycrystalline grain

thickness of the GdO_x film is 14.8 nm (Fig. 2d). Therefore, the thickness of SiO_2 is 40 ± 2 nm and the thickness of GdO_x is 15 ± 0.5 nm. The thicker GdO_x film shows clearly polycrystalline grains and its boundary [29, 30], which will help to detect H_2O_2. Elemental composition of the SiO_2 and GdO_x films is observed by XPS, which is shown in Fig. 3. The peak binding energy of Si*2p* spectra for the S1 sample is 103.35 eV (Fig. 3a), which is similar to the reported value of SiO_2 at 103.58 eV [31]. The spectra are fitted by Shirley background subtraction and Gaussian/Lorentzian functions. The Si*2p* spectrum shows one characteristic peak after de-convolution. Similarly, one characteristic peak of O*1s* centered at 531.5 eV is also observed (Fig. 3d). Lower values of full-width half-maximum (FWHM) are found to be 1.84 and 1.64 eV for the Si*2p* and O*1s* spectra, respectively. The ratio of O:Si is 1.84, which signifies the stoichiometric SiO_2. An XPS spectrum of GdO_x shows Gd$3d_{3/2}$ and Gd$3d_{5/2}$ doublet with binding energy of 1220.5 and 1188.3 eV, respectively (not shown here). However, peak binding energies of Gd$3d_{3/2}$ and Gd$3d_{5/2}$ spin-orbits are reported as 1218 and 1186 eV, respectively [32]. XPS spectra of Gd$3d_{5/2}$ core-level electrons are 1189 eV for S2 (Fig. 3b) and 1188.7 eV for S3 (Fig. 3c) samples, which are identified to be Gd_2O_3 $3d_{5/2}$ or Gd_2O_3 films. Corresponding lower binding energy peaks at 1186.2 and 1185.8 eV indicate the metallic Gd$3d_{5/2}$ peaks for the S2 and S3 samples, respectively. The area ratios of Gd/Gd_2O_3 are found to be 0.64:1 and 0.69:1 for the S2 and S3 samples, respectively, which show higher percentage of Gd in the S3 samples owing to polycrystalline grains. However, the O*1s* core-level spectra show three distinct peaks for the S2 (Fig. 3e) and S3 (Fig. 3f) samples. The strong peaks at 531.5 eV correspond to the oxygen in the Gd_2O_3 film, whereas lower (O*1s* A) and higher (O*1s* B) binding energy peaks centered at 529 and 532.9 eV are attributed to the hydroxyl (OH^-) and carbonate groups in Gd_2O_3 films, respectively [33, 34]. Moreover, the lower binding energy peak corresponds to Gd-O bonding or GdO_x [35]. The area ratios of O*1s* A and O*1s* B with respect to O*1s* are 0.04:1 and 0.48:1 for the S2 samples whereas those values are 0.08:1 and 0.1:1 for the S2 samples, respectively. Therefore, the S2 samples show higher percentage of O*1s* B owing to higher carbonate groups in the GdO_x films, which is insensitive to H_2O_2 sensing. On the other hand, the S3 samples have higher percentage of O*1s*A owing to higher OH^- and higher Gd content in Gd_2O_3 film, i.e., GdO_x film. So, oxygen can be bonded loosely with Gd on a polycrystalline grain boundary as well as a thicker GdO_x film will help to sense H_2O_2, which will be explained below.

Figure 4a shows the C-V characteristics with pH values from 6 to 10 for the S2 and S3 sensors. The V_r values of the S2 sensors are −0.84, −0.75, and −0.63 V for pH 6, 8, and 10, while those values are 0.01, 0.1, and 0.23 V for the S3 sensors, respectively. The V_r values of the S3 sensor are shifted towards the positive direction and are lower than the V_r values of the S2 sensors. This is due to lower oxide charges for the thicker GdO_x membrane (55 vs. 43 nm [36]) and polycrystalline grains with higher OH^- ions (Fig. 3f). The pH sensitivity values are found to be 51.2 and 54.2 mV/pH for the S2 and S3 sensors, respectively, which are higher than the pH sensitivity of approximately 35 mV/pH from pH 2 to 10 [28, 37] and 42 mV/pH from pH 6 to 10 for the S1 sensors. The pH sensitivity of a 30-nm-thick GdO_x membrane is approximately 51.7 mV/pH (not shown C-V curves), which is slightly lower than the S3 sensors. The pH sensitivity value of our GdO_x membrane is comparable with other reported values of 48.29 mV/pH by Wang et al. [27], 64.78 mV/pH by Chang et al. [38], and 55 mV/pH by Yang et al. [39]. However, the S3 sensors show the lowest drift rate as compared to the S1 and S2 sensors (2.12 mV/h vs. 3.12 mV/h and 2.16 mV/h), as shown in Fig. 4b. The drift characteristics were measured a long time up to 500 min at pH 7 buffer solution. Considering a

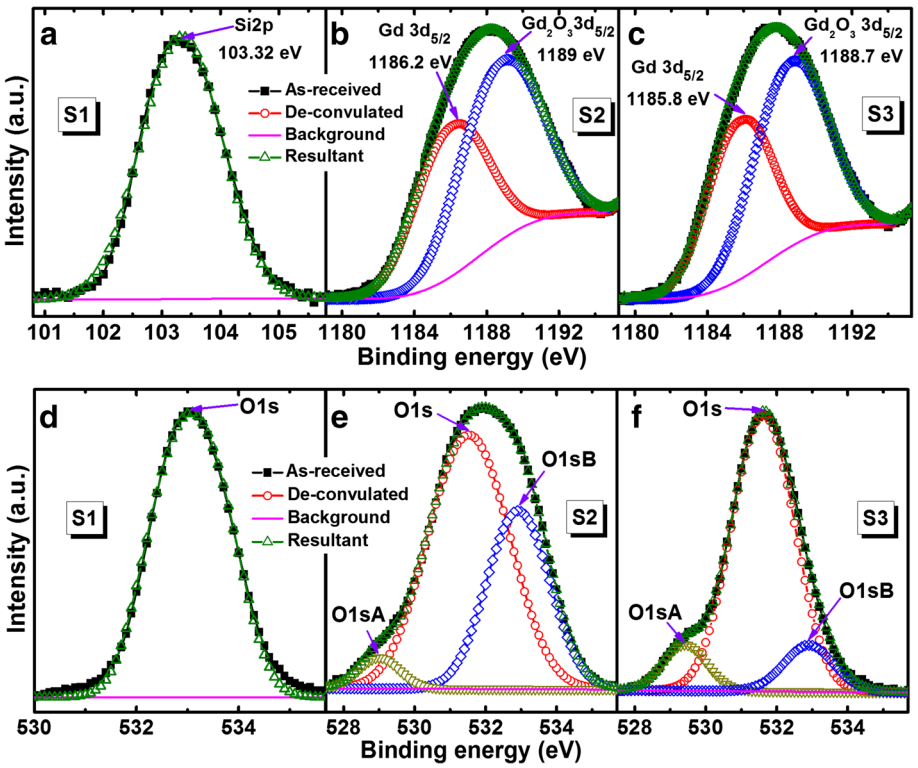

Fig. 3 XPS characteristics of Si*2p* for **a** S1, **b** S2, and **c** S3 samples. Corresponding O*1s* spectra of **d** S1, **e** S2, and **f** S3 samples are shown. The S3 film shows higher Gd/Gd_2O_3 ratio or oxygen deficient and higher OH group which helps to sense H_2O_2

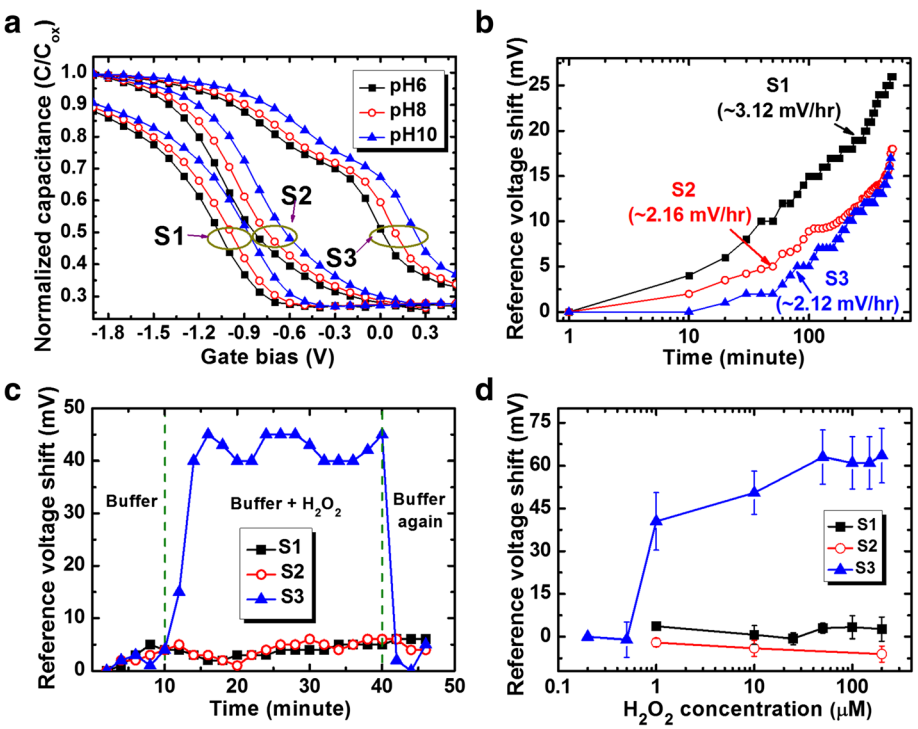

Fig. 4 **a** C-V characteristics of the S1, S2, and S3 sensors are shown. **b** Drift rate characteristics of the S1, S2, and S3 sensors. **c** Time-dependent response of H_2O_2 and **d** reference voltage shift vs. H_2O_2 concentration for all sensors

low drift rate (2.12 mV/h), the pH detection limit of the S3 sensors is 0.039 pH, which is due to high pH sensitivity. It is interesting to note that the GdO_x membrane will detect H_2O_2. Figure 4c shows the time-dependent response of H_2O_2 for the S3 sensors. A negligible V_r shift is observed for pH 7 buffer solution up to 10 min. By including H_2O_2 with a concentration of 1 μM, a good V_r shift of approximately 40 mV is observed because of Gd^{1+}, Gd^{2+}, and Gd^{3+} oxidation states (https://en.wikipedia.org/wiki/Work_function) [40]. On the other hand, both S1 and S2 sensors do not show H_2O_2 sensing. When in contact with H_2O_2, the Gd^{2+} changes to the Gd^{3+} oxidation state and provides electrons for the reduction of H_2O_2. H_2O as a byproduct is observed (Fig. 1). However, the pH value is unchanged by adding H_2O_2 in the buffer solution. A short response time of <2 min is needed without enzyme. After washing out, the sensor does not show any V_r shift owing to the reduction from the Gd^{3+} to Gd^{2+} states. Therefore, this sensor can be used repeatedly for H_2O_2 sensing. Based on our knowledge, this is the first ever report of H_2O_2 detection with a polycrystalline GdO_x membrane. Basically, the oxidation/reduction of the GdO_x material in contact with H_2O_2 with buffer solutions is responsible for the V_r shifting, which is shown by chemical reactions below.

$$\mathrm{Gd} \leftrightarrow \mathrm{Gd}^{2+} + 2e^- \leftrightarrow \mathrm{Gd}^{3+} + 3e^- \quad (1)$$

$$\mathrm{H_2O_2} + e^- \leftrightarrow \mathrm{OH}^- + \mathrm{OH}^* \quad (2)$$

$$\mathrm{OH}^* + e^- \leftrightarrow \mathrm{OH}^- \quad (3)$$

$$2\mathrm{OH}^- + 2\mathrm{H}^+ \leftrightarrow 2\mathrm{H_2O} \quad (4)$$

By following the above Eqs. (1), (2), (3), and (4), the oxidation state of Gd changes from Gd^{2+} to Gd^{3+}. The H^+ ions are supplied by buffer solutions. The V_r shift increases with increasing H_2O_2 concentration from 1 to 200 μM because the generation of Gd^{3+} ions increases (Fig. 4d). A moderate sensitivity of 0.13 mV/μM is obtained from a linear range of 1 to 200 μM whereas it is 82 mV/μM from a linear range of 0.5 to 1 μM. Our detection limit of 1 μM is inferior than the published results [9–12, 15, 16, 41–43], comparable with the published results [44–47], and superior than the published results [13, 17, 18, 20, 48–52] in literature by using different sensing methods, as shown in Table 1. Further study is needed to improve the detection limit in the future. However, our sensing method's surface potential is changed when in contact with H_2O_2 because of the catalytic activity of Gd. It is known that Gd_2O_3 material is n-type and the energy difference in between the Fermi level and the conduction band (E_c) is 2.71 eV [53]. The electron affinity of Gd_2O_3 is 1.45 eV by considering the conduction band offset of 2.6 eV with Si [54]. The work function of Gd increases from 2.9 eV (https://en.wikipedia.org/wiki/Work_function) to 4.16–4.76 eV [53–55] after oxidation. This suggests that the work function of GdO_x is modulated by oxidation/reduction or Gd^{3+} concentration as well as the energy band bending of Si is changed. In consequence, the V_r is needed to bring Si energy bands to be flat. On the other hand, the S1 and S2 sensors do not show H_2O_2 detection because they do not have redox properties. The thinner GdO_x film (S2) has a smaller crystalline grain with less Gd content (Fig. 3), while the S3 sensor has larger crystalline grain (Fig. 5a) with higher Gd content. Figure 5b shows electron energy loss spectroscopy of Gd measured at polycrystalline grain (P_1) and amorphous region or grain boundary (P_1). The regions of P_1 and P_2 are marked on Fig. 5a. The edges of the Gd M-4 and M-5 peaks at the P_1 region are located at 1216.8 and 1187.5 eV, while those values at the P_2 region are 1216.5 and 1187 eV, respectively. Du et al. [56] have reported the M-4 and M-5 peak values of 1217 and 1185 eV for the $Gd(OH)_3$ nanorods. The edges of the O-K

Table 1 Comparison of linear range and detection limit of H_2O_2 published in literature [9–13, 15–18, 20, 41–52]

Sensing materials	pH value	Linear range (μM)	Detection limit (μM)
MoS_2 NP [15]	7.4	5–100	0.002
WS_2 NS [10]	7.4	–	0.002
Pt-Pd-Fe_3O_4 [16]	7.4	0.02–0.1, 2–14,000	0.005
Pt-Pd/rGO [11]	7.0	0.1–37.6	0.01
Au NP [12]	7.0	2–5000	0.01
Pt NP [9]	7.2	3–300	0.03
rGO [41]	7.0	0.05–1500	0.05
Au/C/Pt [42]	7.0	9.0–1860, 1860–7110	0.13
Au NP [43]	6.8	3–605	0.18
Ag NP [44]	7.5	100–10,000	0.88
GS/CeO_2-ZnO NP [45]	7.0	2–20,000	1.1
Pt-Pd and Pt-Ir [46]	7.4	2.5–125	1.2
Pt NP [47]	6.9	5–2000	1.23
CeO_2 NP/N-rGO [48]	7.0	1.8–920.8	1.3
CuO [13]	7.0	10–13,180	1.6
Ag NPs/PPy/Fe_3O_4 [49]	7.2	5–11,500	1.7
Pd NP [17]	7.4	2–1300	2
Co_3O_4 NW [18]	7.4	15–675	2.4
Carbon dots [20]	7.4	3–300	3
Se/Pt [50]	7.0	10–15,000	3.1
Ag NP [51]	7.0	25–500, 500–5500	10
Co-Mn [52]	7.2	100–25,000	15
GdO_x in EIS structure (this work)	7.0	1–200	1

NP nanoparticle, *NS* nanosheet, *rGO* reduced graphene oxide, *GS* graphene sheet, *NW* nanowire

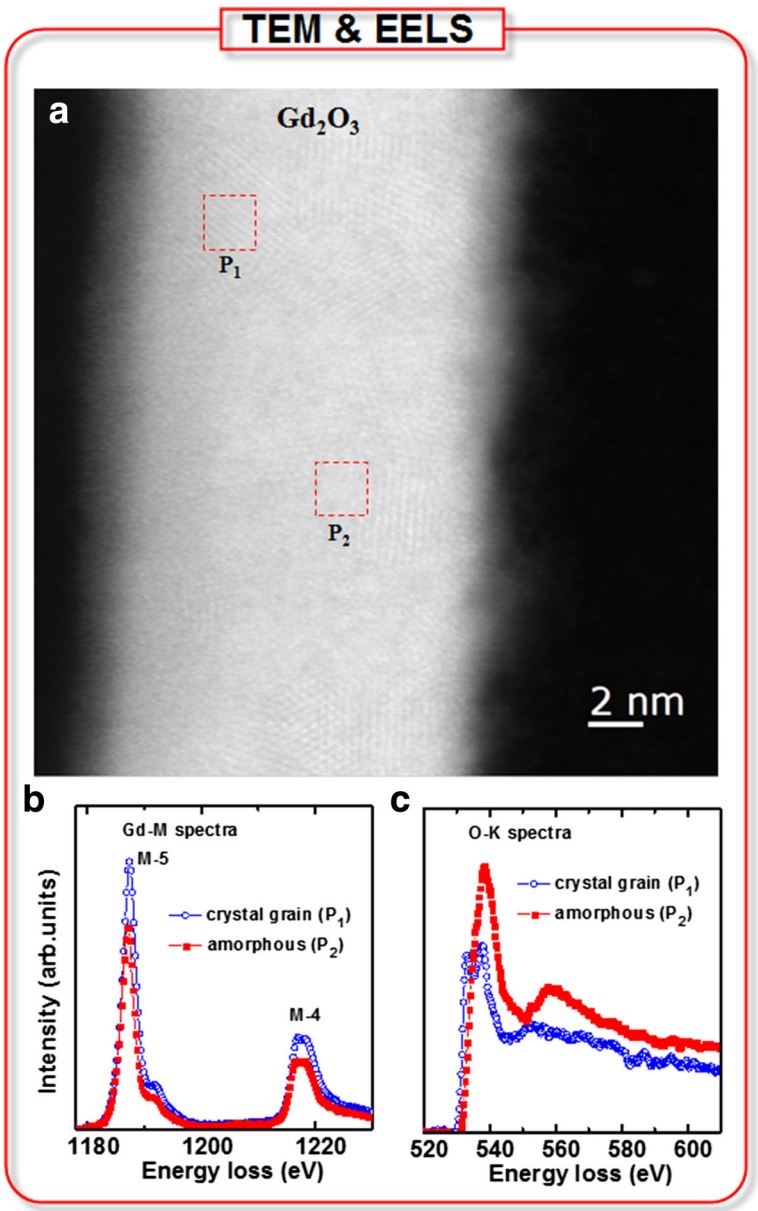

Fig. 5 **a** TEM image for EELS spectra of the S3 membranes. The edges of **b** Gd and **c** O-K are plotted for the P_1 and P_2 regions marked on a. The polycrystalline grain corresponds to Gd^{2+} and the grain boundary corresponds to Gd^{3+} oxidation states

peak at both P_1 and P_2 regions are located at 538.5 eV, as shown in Fig. 5c, which is close to the reported value of 536.5 eV [56]. It is interesting to note that another peak of crystalline grain (P_1) is located at 532.9 eV, which is shifted downwards to 3.9 eV. Egerton has reported the reduced energy gap of SiO_x at the SiO_2/Si interface with energy shift downwards to 3 eV [57]. In our case, this reduced energy gap is observed in the polycrystalline grain region. Therefore, the crystalline grain is GdO_x (or Gd^{2+}) and the amorphous region or grain boundary is Gd_2O_3 (or Gd^{3+}). When in contact with H_2O_2, the oxidation state of the S3 sensor changes from Gd^{2+} to Gd^{3+} and the crystalline grain takes a major role, which is confirmed by EELS spectra. So, the thicker crystalline GdO_x membrane can sense H_2O_2 repeatedly which will be useful to detect human disease in the near future.

Conclusions

Higher pH sensitivity (54.2 m/pH) and the enzyme-free H_2O_2 sensing characteristics have been investigated by using 15-nm-thick GdO_x membranes for the first time. The polycrystalline grain and thickness of the GdO_x/SiO_2 film have been observed by TEM image. XPS characteristics of the S3 membrane show higher Gd/Gd_2O_3

ratio than the S2 membrane (0.69/1 vs. 0.64/1). The S3 membrane shows GdO_x and higher OH content in the crystalline grain, which help to sense H_2O_2 whereas both S1 and S2 sensors do not show H_2O_2 detection. Therefore, a larger polycrystalline GdO_x grain has oxidation/reduction properties when in contact with H_2O_2, which is confirmed by EELS. During oxidation, the Gd^{2+} changes to the Gd^{3+} state and the amount of Gd^{3+} ions increases with increasing H_2O_2 concentration from 1 to 200 μM. A low defection limit of 1 μM is obtained owing to the catalytic effect of Gd. The time-dependent response and the sensing mechanism of H_2O_2 have been explored. Due to the short time detection of H_2O_2 in the EIS structure, this novel GdO_x sensing membrane paves a way to diagnose other diseases of the human body in the near future.

Acknowledgements
This work was supported by the Ministry of Science and Technology (MOST), Taiwan, under contract numbers MOST-104-2221-E-182-075 and MOST-105-2221-E-182-002 and Chang Gung Memorial Hospital (CGMH), Linkou, under contract numbers CMRPD270021 and CMRPD2E0091. The authors are grateful to Mr. S. Chatterjee for the partial support to measure the concentration-dependent hydrogen peroxide sensing.

Authors' Contributions
PK fabricated these sensors and analyzed the data under the instruction of SM. JTQ helped to analyze the sensing mechanism and application of this sensor. SJ and AR helped to measure the pH and H_2O_2 sensing characteristics and checked the repeatability of these sensors. They review the papers under the instruction of SM. KS helped to check the redox characteristics and review the papers under the instruction of SM. HMC measured the XPS and analyzed the spectra. MTC helped to obtain TEM and EELS. RM helped to analyze the sensing characteristics. HCC helped to deliver the idea for deposition of sensing membrane by using electron beam evaporation. JRY analyzed the EELS spectra for oxidation and reduction. All authors contributed to the revision of the manuscript, and they approved it for publication.

Competing Interests
The authors declare that they have no competing interests.

Author details
[1]Department of Electronic Engineering, Chang Gung University (CGU), 259 Wen-Hwa 1st Rd., Kwei-Shan, Tao-Yuan 333, Taiwan. [2]Bio-Sensor Lab., Biomedical Engineering Research Center, Department of Electronic Engineering, Chang Gung University, Tao-Yuan 333, Taiwan. [3]Center for Reliability Science and Technologies (CReST), Department of Electronic Engineering, Chang Gung University, Tao-Yuan 333, Taiwan. [4]Department of Biomedical Sciences, School of Medicine, Chang Gung University (CGU), Tao-Yuan 333, Taiwan. [5]Division of Gyn-Oncology, Department of Obs/Gyn, Chang Gung Memorial Hospital (CGMH), Tao-Yuan 333, Taiwan. [6]Material and Chemical Research Laboratories (MRL), Industrial Technology Research Institute (ITRI), Hsinchu 195, Taiwan. [7]Department of Electronics and Communications Engineering, National Institute of Technology (NIT), Durgapur 713209, India. [8]Department of Materials Science and Engineering, National Taiwan University (NTU), Taipei 106, Taiwan.

Received: 13 August 2016 Accepted: 22 September 2016
Published online: 29 September 2016

References

1. Chen X, Wu G, Cai Z, Oyama M, Chen X (2014) Advances in enzyme-free electrochemical sensors for hydrogen peroxide, glucose, and uric acid. Microchim Acta 181:689
2. Wang J, Chen XJ, Liao KM, Wang GH, Han M (2015) Pd nanoparticle-modified electrodes for nonenzymatic hydrogen peroxide detection. Nanoscale Res Lett 10:311
3. Nulton-Persson AC, Szweda LI (2001) Modulation of mitochondrial function by hydrogen peroxide. J Biol Chem 276:23357
4. Veal EA, Day AM, Morgan BA, Morgan D (2007) Hydrogen peroxide sensing and signaling. Mol Cell 26:1
5. Rhee SG, Chang TS, Jeong W, Kang D (2010) Methods for detection and measurement of hydrogen peroxide inside and outside of cells. Mol Cell 29:539
6. Chen S, Yuan R, Chai Y, Hu F (2013) Electrochemical sensing of hydrogen peroxide using metal nanoparticles: a review. Microchim Acta 180:15
7. Chen W, Cai S, Ren QQ, Wen W, Zhao YD (2012) Recent advances in electrochemical sensing for hydrogen peroxide: a review. Analyst 137:49
8. Li L, Du Z, Liu S, Hao Q, Wang Y, Li Q, Wang T (2010) A novel nonenzymatic hydrogen peroxide sensor based on MnO_2/graphene oxide nanocomposite. Talanta 82:1637
9. Zhang M, Liao C, Mak CH, You P, Mak CL, Yan F (2016) Highly sensitive glucose sensors based on enzyme-modified whole-graphene solution-gated transistors. Sci Rep 5:1
10. Tang J, Quan Y, Zhang Y, Jiang M, Al-Enizi AM, Kang B, An T, Wang W, Xia L, Gong X, Zheng G (2016) Three-dimensional WS_2 nanosheet networks for H_2O_2 produced for cell signaling. Nanoscale 8:5786
11. Sun Y, Zheng H, Wang C, Yang M, Zhou A, Duan H (2016) Ultrasonic-electrodeposition of PtPd alloy nanoparticles on ionic liquid-functionalized graphene paper: towards a flexible and versatile nanohybrid electrode. Nanoscale 8:1523
12. Vilian TE, Veeramani V, Chen S-M, Madhu R, Kwak CH, Huh YS, Han YK (2015) Immobilization of myoglobin on Au nanoparticle-decorated carbon nanotube/polytyramine composite as a mediator-free H_2O_2 and nitrite biosensor. Sci Rep 5:18390
13. Huang J, Zhu Y, Zhong H, Yang X, Li C (2014) Dispersed CuO nanoparticles on a silicon nanowire for improved performance of nonenzymatic H_2O_2 detection. ACS Appl Mater Interfaces 6:7055
14. Maji SK, Mandal AK, Nguyen KT, Borah P, Zhao Y (2015) Cancer cell detection and therapeutics using peroxidase-active nanohybrid of gold nanoparticle-loaded mesoporous silica-coated graphene. ACS Appl Mater Interfaces 7:9807
15. Wang T, Zhu H, Zhuo J, Zhu Z, Papakonstantinou P, Lubarsky G, Lin J, Li M (2013) Biosensor based on ultrasmall MoS_2 nanoparticles for electrochemical detection of H_2O_2 released by cells at the nanomolar level. Anal Chem 85:10289
16. Sun X, Guo S, Liu Y, Sun S (2012) Dumbbell-like PtPd–Fe_3O_4 nanoparticles for enhanced electrochemical detection of H_2O_2. Nano Lett 12:4859
17. Liu Y, Sun G, Jiang C, Zheng XT, Zheng L, Li CM (2014) Highly sensitive detection of hydrogen peroxide at a carbon nanotube fiber microelectrode coated with palladium nanoparticles. Microchim Acta 181:63
18. Kong L, Ren Z, Zheng N, Du S, Wu J, Tang J, Fu H (2015) Interconnected 1D Co_3O_4 nanowires on reduced graphene oxide for enzymeless H_2O_2 detection. Nano Res 8:469
19. Hao C, Shen Y, Wang Z, Wang X, Feng F, Ge C, Zhao Y, Wang K (2016) Preparation and characterization of Fe_2O_3 nanoparticles by solid phase method and its hydrogen peroxide sensing properties. ACS Sustainable Chem Eng 4:1069
20. Bai J, Sun C, Jiang X (2016) Carbon dots-decorated multiwalled carbon nanotubes nanocomposites as a high-performance electrochemical sensor for detection of H_2O_2 in living cells. Anal Bioanal Chem 408:4705
21. Zhang M, Wang Z (2013) Nanostructured silver nanowires-graphene hybrids for enhanced electrochemical detection of hydrogen peroxide. Appl Phys Lett 102:213104
22. Zhan B, Liu C, Shi H, Li C, Wang L, Huang W, Dong X (2014) A hydrogen peroxide electrochemical sensor based on silver nanoparticles decorated three-dimensional grapheme. Appl Phys Lett 104:243704
23. Oha JY, Jang HJ, Cho WJ, Islam MS (2012) Highly sensitive electrolyte-insulator-semiconductor pH sensors enabled by silicon nanowires with Al_2O_3/SiO_2 sensing membrane. Sens Actuators B 171–172:238
24. Schoning MJ, Brinkmann D, Rolka D, Demuth C, Poghossian A (2005) CIP (cleaning-in-place) suitable 'non-glass' pH sensor based on a Ta_2O_5- gate EIS structure. Sens Actuators B 111–112:423
25. Lu TF, Chuang HC, Wang JC, Yang CM, Kuo PC, Lai CS (2011) Effects of thickness effect and rapid thermal annealing on pH sensing characteristics of thin HfO_2 films formed by atomic layer deposition. Jpn J Appl Phys 50:1

26. Yang HW, Huang CY, Lin CW, Liu HL, Huang CW, Liao SS, Chen PY, Lu YZ, Wei KC, Ma CC (2014) Gadolinium-functionalized nanographene oxide for combined drug and microRNA delivery and magnetic resonance imaging. Biomaterials 35(24):6534. doi:10.1016/j.biomaterials.2014.04.057
27. Wang JJ, Lin SR, Kao CH, Hu CH, Chen H (2015) Electrolyte-insulator-semiconductor (EIS) with Gd_2O_3-based sensing membrane for pH sensing application. J New Mat Electrochem Syst 18:1
28. Kumar P, Maikap S, Prakash A, Tien TC (2014) Time-dependent pH sensing phenomena using CdSe/ZnS quantum dots in EIS structure. Nanoscale Res Lett 9:179
29. Manna S, Aluguri R, Katiyar A, Das S, Laha A, Osteen HJ, Ray SK (2013) MBE-grown Si and $Si_{1-x}Ge_x$ quantum dots embedded within epitaxial Gd_2O_3 on Si (111) substrate for floating gate memory device.Nanotechnology 24:505709
30. Mahapatra R, Maikap S, Lee JH, Kar GS, Dhar A, Hwang NM, Kim DY, Mathur BK, Ray SK (2003) Effects of interfacial nitrogen on the structural and electrical properties of ultrathin ZrO_2 gate dielectrics on partially strain compensated SiGe/Si heterolayers. Appl Phys Lett 82:4331
31. Jana D, Dutta M, Samanta S, Maikap S (2014) RRAM characteristics using a new Cr/GdO_x/TiN structure. Nanoscale Res Lett 9:680
32. Ahren M, Selegard L, Klasson A, Soderlind F, Abrikossova N, Skoglund C, Bengtsson T, Engstrom M, Kall PO, Uvda K (2010) Synthesis and characterization of PEGylated Gd_2O_3 nanoparticles for MRI contrast enhancement. Langmuir 26:5753
33. Majeeda S, Shivashankar SA (2014) Rapid, microwave-assisted synthesis of Gd_2O_3 and Eu:Gd_2O_3 nanocrystals: characterization, magnetic, optical and biological studies. J Mater Chem B 2:5585
34. Khan SA, Gambhir S, Absar A (2014) Extracellular biosynthesis of gadolinium oxide (Gd_2O_3) nanoparticles, their bio-distribution and bio-conjugation with the chemically modified anticancer drug taxol. J Nanotechnol 5:249
35. Cho HK, Cho HJ, Lone S, Kim DD, Yeum JH, Cheong IW (2011) Preparation and characterization of MRI-active gadolinium nanocomposite particles for neutron capture therapy. J Mater Chem 21:15486
36. Duenas S, Castan H, Garcia H, Gomez A, Bailon L, Kukli K, Hatanpaa T, Lu J, Ritala M, Leskela M (2007) Electrical properties of atomic-layer-deposited thin gadolinium oxide high-k gate dielectrics. J Electrochem Soc 154:G207
37. Maikap S, Prakash A, Banerjee W, Das A, Lai CS (2010) Characteristics of pH sensors fabricated by using protein mediated CdSe/ZnS quantum dots. Microelectron Reliab 50:747
38. Chang LB, Ko HH, Jeng MJ, Lee YL, Lai CS (2007) pH-sensitive Gd_2O_3 / SiO_2 stacked capacitors prepared by pure water anodic oxidation. J Electrochem Soc 154:J150
39. Yang CM, Wang CY, Lai CS (2014) Characterization on pH sensing performance and structural properties of gadolinium oxide post-treated by nitrogen rapid thermal annealing. J Vac Sci Technol B 32:03D113
40. Hong M (1999) Epitaxial cubic gadolinium oxide as a dielectric for gallium arsenide passivation. Science 283:1897
41. Zhou M, Zhai Y, Dong S (2009) Electrochemical sensing and biosensing platform based on chemically reduced graphene oxide. Anal Chem 81:5603
42. Zhang Y, Li Y, Jiang Y, Li Y, Li S (2016) The synthesis of Au@C@Pt core-double shell nanocomposite and its application in enzyme-free hydrogen peroxide sensing. Appl Surf Sci 378:375
43. Bao S, Du M, Zhang M, Zhu H, Wang P, Yang T, Zou M (2014) Fabrication of gold nanoparticles modified carbon nanofibers/polyaniline electrode for H_2O_2 determination. J Electrochem Soc 161:H816
44. Wu Z, Yang S, Chen Z, Zhang T, Guo T, Wang Z, Liao F (2013) Synthesis of Ag nanoparticles-decorated poly(m-phenylenediamine) hollow spheres and the application for hydrogen peroxide detection. Electrochim Acta 98:104
45. Yang X, Wu F, Ouyang Y, Hu Y, Zhang H, Ji Y (2016) Zinc oxide nanoparticles decorated on graphene sheets@cerium oxide nanocomposites to sensitize gold electrode for the nonenzymatic hydrogen peroxide detection. J Electrochem Soc 163:H834
46. Chen KJ, Pillai KC, Rick J, Pan CJ, Wang CH, Liu CC, Hwang BJ (2012) Bimetallic PtM (M = Pd, Ir) nanoparticle decorated multi-walled carbon nanotubes enzyme-free, mediator-less amperometric sensor for H_2O_2. Biosens Bioelectron 33:120
47. Niu X, Zhao H, Chen C, Lan M (2012) Platinum nanoparticle-decorated carbon nanotube clusters on screen-printed gold nanofilm electrode for enhanced electrocatalytic reduction of hydrogen peroxide. Electrochim Acta 65:97
48. Yang S, Li G, Wang G, Liu L, Wang D, Qu L (2016) Synthesis of highly dispersed CeO_2 nanoparticles on N-doped reduced oxide graphene and their electrocatalytic activity toward H_2O_2. J Alloy Compd 688:910
49. Qi C, Zheng J (2015) Novel nonenzymatic hydrogen peroxide sensor based on Fe_3O_4/PPy/Ag nanocomposites. J Electroanal Chem 747:53
50. Li Y, Zhang JJ, Xuan J, Jiang LP, Zhu JJ (2010) Fabrication of a novel nonenzymatic hydrogen peroxide sensor based on Se/Pt nanocomposites. Electrochem Commun 12:777
51. Roof BR, Ojani R, Hasheminejad E, Rashid-Nadimi S (2012) Electrochemical synthesis of Ag nanoparticles supported on glassy carbon electrode by means of p-isopropyl calix[6]arene matrix and its application for electrocatalytic reduction of H_2O_2. Appl Surf Sci 258:2788
52. Kuo CC, Lan WJ, Chen CH (2014) Redox preparation of mixed-valence cobalt manganese oxide nanostructured materials: highly efficient noble metal-free electrocatalysts for sensing hydrogen peroxide. Nanoscale 6:334
53. Chiu YP, Huang BC, Shih MC, Shen JY, Chang P, Chang CS, Huang ML, Tsai M-H, Hong M, Kwo J (2011) Atomic-scale determination of band offsets at the Gd_2O_3/GaAs (100) hetero-interface using scanning tunneling spectroscopy. Appl Phys Lett 99:212101
54. Fissel A, Czernohorsky M, Osten HJ (2006) Growth and characterization of crystalline gadolinium oxide on silicon carbide for high-application superlattices. Microstruct 40:551
55. Lipp E, Shahar Z, Bittel BC, Lenahan PM, Schwendt D, Osten HJ, Eizenberg M (2011) Trap-assisted conduction in Pt-gated Gd_2O_3/Si capacitors. J Appl Phys 109:073724
56. Du G, Tendeloo GV (2005) Preparation and structure analysis of $Gd(OH)_3$ nanorods. Nanotechnology 16:595
57. Egerton RF (2009) Electron energy-loss spectroscopy in the TEM. Rep Prog Phys 72:016502